

Supporting Information

Adsorption Processes on a Pd Monolayer-modified Pt(111) Electrode

Xiaoting Chen,^{#a} Laura P. Granda-Marulanda,^{#a} Ian T. McCrum^a and Marc T.M. Koper^{*a}

^aLeiden Institute of Chemistry, Leiden University, PO Box 9502, 2300 RA, Leiden, the Netherlands

[#]Both authors contributed equally; ^{*}m.koper@chem.leidenuniv.nl

Contents

S1. Experimental	3
S2. Computational methods	8
Gibbs Free Energy of Adsorption	9
Adsorption free energies of * OH, *H and *O	11
Free energies vs. coverage diagrams	15
References	17

S1. Experimental

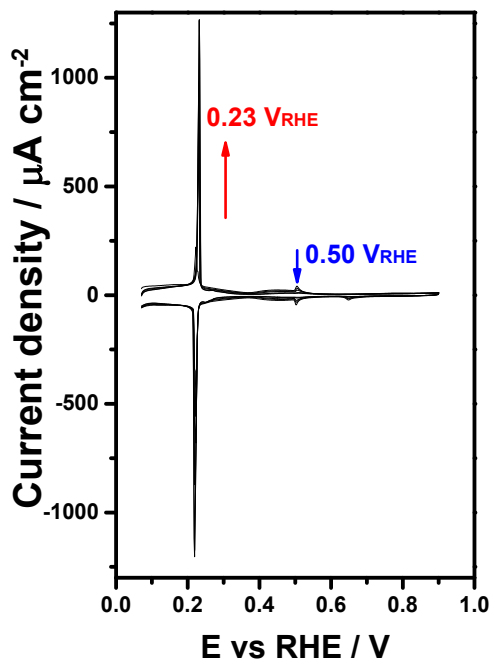


Figure S1. Electrochemical deposition of palladium monolayer on Pt(111) electrode from 0.1 M H_2SO_4 + 0.1 mM PdSO_4 . Scan rate: 50 mV s^{-1} . Arrows indicate the evolution with time.

Figure S1 shows the effect of the progressive accumulation of palladium on the Pt(111) electrode surface on the voltammetric profile of the electrode during the electrochemical deposition of palladium monolayer. Initially, the presence of palladium on the surface is reflected in the growth of a sharp adsorption state at $0.23 \text{ V}_{\text{RHE}}$, simultaneously with the progressive decrease of the characteristic adsorption states of Pt(111) in 0.1 M H_2SO_4 . In addition, the presence of the characteristic spike of Pt(111) at $0.50 \text{ V}_{\text{RHE}}$ strongly suggests the existence of wide Pt(111) domains. With increasing deposition cycles the last contributions from the Pt(111) domains around $0.50 \text{ V}_{\text{RHE}}$ disappear. Previous studies using scanning tunnelling microscopy (STM) showed a complete pseudomorphic monolayer of Pd is formed prior to bulk deposition during electrochemical deposition of Pd on Pt(111).¹ The voltammetric charge of (bi)sulfate adsorption at $0.23 \text{ V}_{\text{RHE}}$ can be related in a quantitative

way to the palladium coverage and corresponds to a charge value of $320 \mu\text{C cm}^{-2}$ for $\text{Pd}_{\text{ML}}\text{Pt}(111)$.²

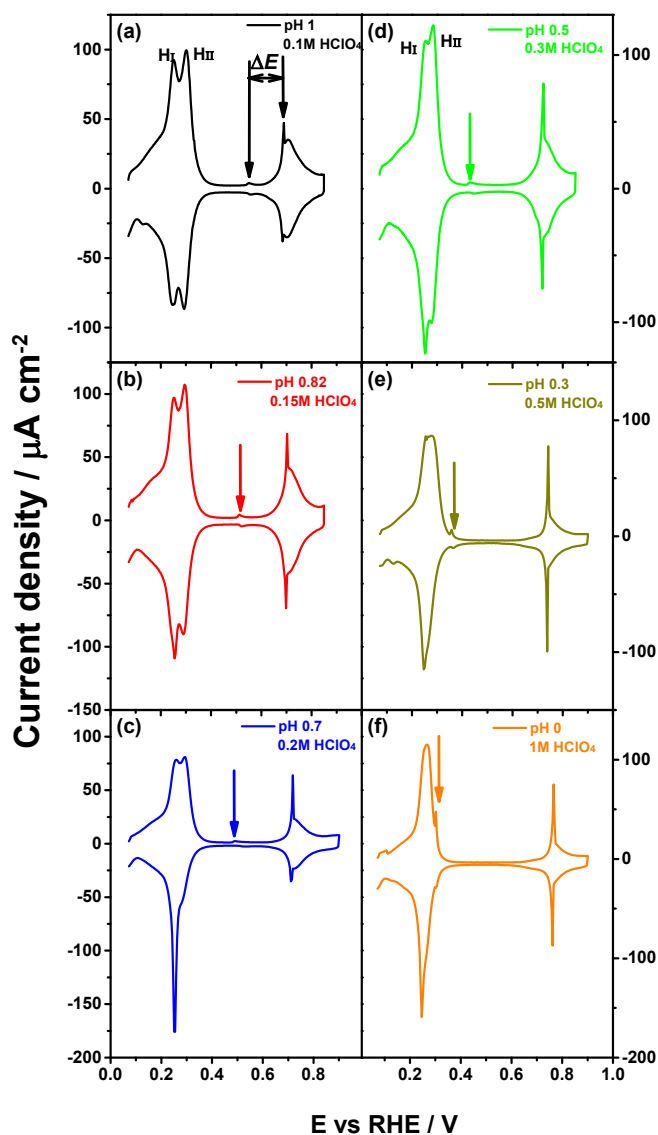


Figure S2. Cyclic voltammogram of $\text{Pd}_{\text{ML}}\text{Pt}(111)$ electrode recorded in (a) 0.1 M HClO_4 (pH=1), (b) 0.15 M HClO_4 (pH=0.82), (c) 0.2 M HClO_4 (pH=0.7), (d) 0.3 M HClO_4 (pH=0.5), (e) 0.5 M HClO_4 (pH=0.3) and (f) 1 M HClO_4 (pH=0). Scan rate: 50 mV s^{-1} .

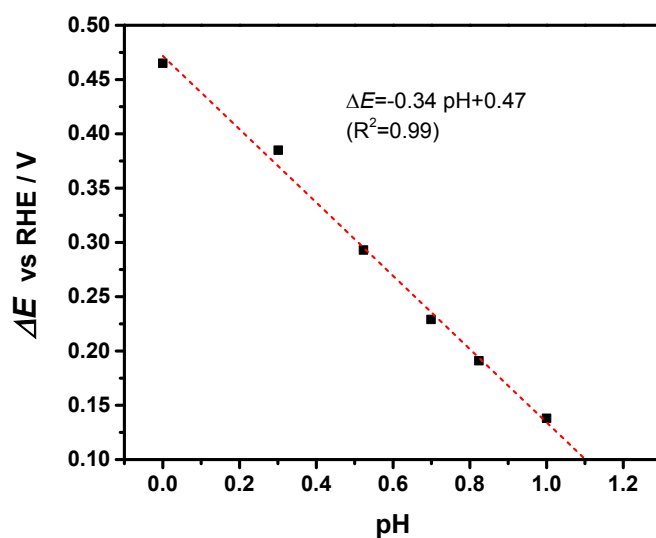


Figure S3. Plot of the peak potential difference ($\square E$) between the small peak (see the two arrows in Figure S2a) and the phase transition peak corresponding to the electrolyte pH.

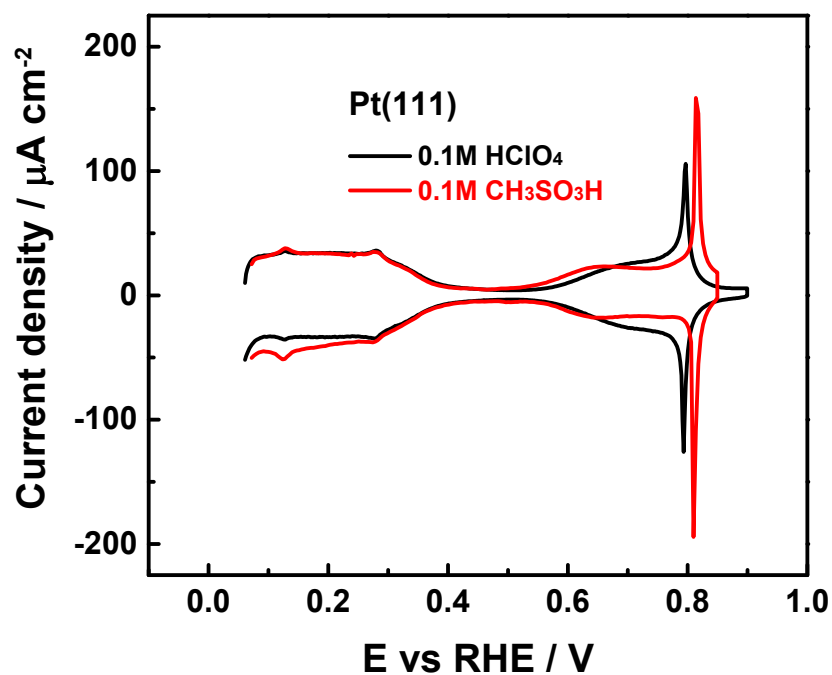


Figure S4. Cyclic voltammogram of Pt(111) electrode recorded in 0.1 M HClO₄ and 0.1 M CH₃SO₃H. Scan rate: 50 mV s⁻¹.

Figure S4 compares the cyclic voltammograms of Pt(111) electrode recorded in 0.1 M HClO₄ and 0.1 M CH₃SO₃H. At potentials lower than 0.55 V_{RHE}, where the hydrogen adsorption/desorption and the double layer regions take place, there is an almost perfect coincidence between both curves. However, at higher potentials, when the adsorption of oxygen-containing species occurs, visible differences between both CVs appear. At 0.55 to 0.90 V_{RHE}, where adsorption of hydroxyl from water dissociation is expected, OH adsorption starts at slightly lower potentials in CH₃SO₃H than in HClO₄ and this could suggest weaker specific adsorption of methylsulfonate as compared with perchlorate. In contrast, the following sharp peak, the spike of the so-called “butterfly” feature, is slightly shifted to higher potentials in 0.1 M CH₃SO₃H.

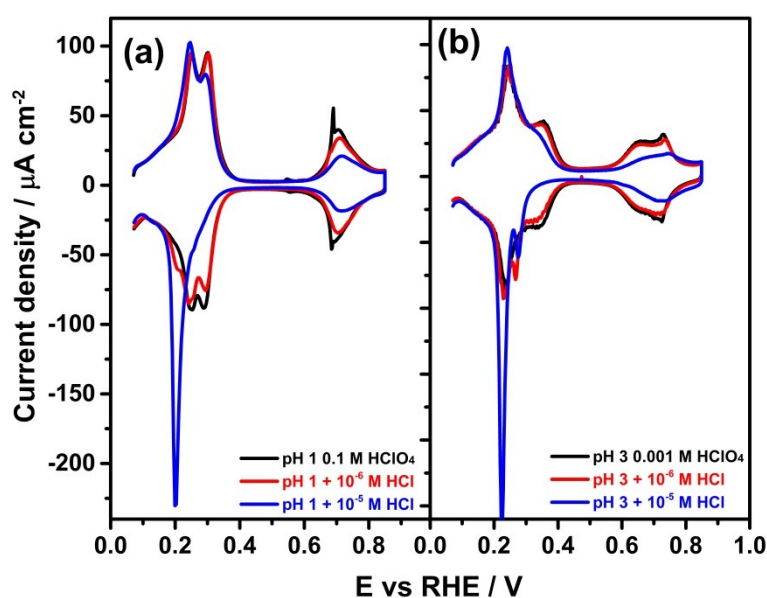


Figure S5. Cyclic voltammogram of Pd_{ML}Pt(111) electrode recorded in (a) 0.1 M HClO₄ (pH=1) and (b) 0.001 M HClO₄ (pH=3), without and with different concentration of Cl⁻. Scan rate: 50 mV s⁻¹.

Figure S5 shows the cyclic voltammograms of the Pd_{ML}Pt(111) electrode recorded in (a) 0.1 M HClO₄ (pH=1) and (b) 0.001 M HClO₄ (pH=3) with small amounts (10⁻⁶ and 10⁻⁵ M) of the

Cl⁻. The change caused by Cl⁻ is the same as reported by Markovic et al³: the observed H_I and H_{II} peaks exhibit asymmetry, in contrast to the symmetrical peaks observed in solutions containing only HClO₄. Therefore, chloride is in competition with the H_{upd} as well as with OH_{ads}.

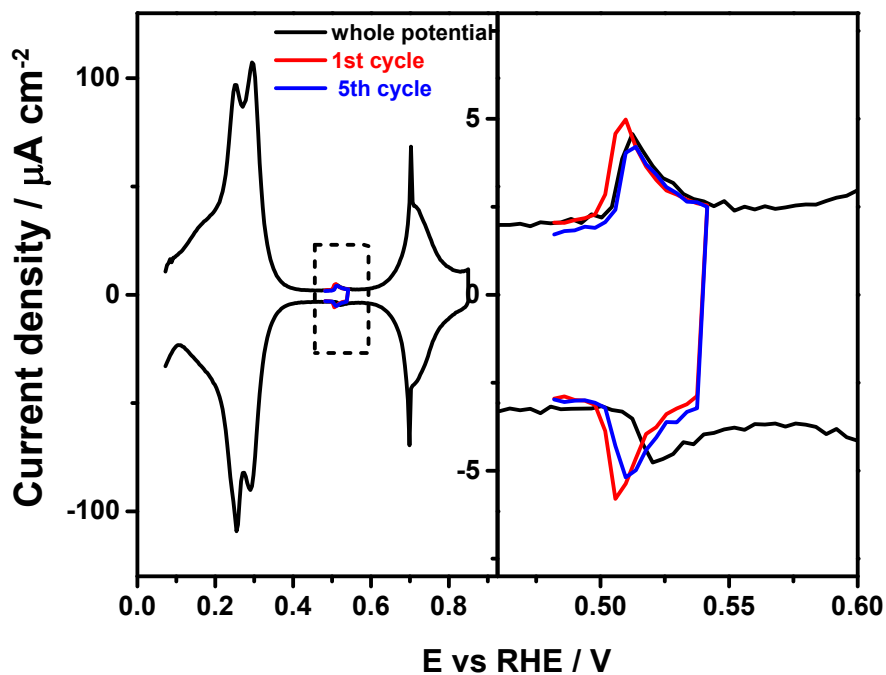


Figure S6. Cyclic voltammograms (the 1st and 5th cycle) of Pd_{ML}Pt(111) when the potential is continuously cycled between 0.48 and 0.54 V_{RHE} in 0.15 M HClO₄. Scan rate: 50 mV s⁻¹. The right panel represents a magnification of the rectangular marked window in the left panel. The cyclic voltammogram of Pd_{ML}Pt(111) in the whole potential window recorded under identical condition is shown for comparison as the black curve.

Figure S6 shows that the small peak in the double layer region is reversible when the potential is continuously cycled between 0.48 and 0.54 V_{RHE}, in contrast to the hysteresis observed using the whole potential window.

S2. Computational methods

All of the calculations were performed using the Vienna Ab initio Simulation Package (VASP)⁴ with the Generalized Gradient Approximation (GGA) PBE exchange correlation functional⁵ and the projector-augmented-wave (PAW) method.⁶ The plane wave energy cut-off was 450 eV. Pt (111) and Pd_{ML}Pt(111) surfaces were modeled using a slab consisting of a (3x3) unit cell. After verifying energy convergence with respect to atomic layers we decided to use 6 atomic layers for Pd_{ML}Pt(111) and Pt(111), in this way providing a convergence criterion of adsorption energies to ≤ 0.05 eV. The k-point sampling grids used for both surfaces were (6 x 6 x 1) using Monkhorst-Pack grids.⁴⁻⁷

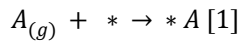
To simulate the bulk, the first two atomic layers were kept fixed at the PBE optimized lattice constant of Pt (3.98 Å) while the remaining atomic layers were relaxed. We include empirical van der Waals (vdW) corrections through the DFT-D3(BJ)^{8,9} method on PBE, here denoted as PBED3, to the calculations for a comparison of the energetics of the water-water and water-metal interaction. The relaxations to find the ground state configurations were made using the quasi-Newton algorithm. Site analysis and geometry optimizations were performed until the forces were smaller than 0.02 eV/Å. To prevent interaction between the slabs along the z axis a vacuum of ~15.0 Å was set for all cases and dipole corrections were also applied by adding the tags LDIPOL= .TRUE., IDIPOL = 3. The slab was positioned at the bottom of the cell, in this way assuring convergence when using the dipole moment corrections. Several attempts with the cell positioned in the center plus dipole corrections failed to converge.

For the surfaces and adsorbed species, the method of Methfessel-Paxton¹⁰ to the second order was used to set the partial occupancies on each orbital and the smearing width was set to 0.2 eV. For the individual molecules a Gaussian smearing with a width of 0.001 eV was used

instead. The gas phase molecules, H₂O(g), H₂(g), ClO₂(g), F₂(g) and SO₂(g) were simulated in an asymmetric box of (15.0 x 15.1 x 15.3) Å at the gamma point 1x1x1.

Gibbs Free Energy of Adsorption

The change in free energies of adsorption were calculated using the hypothetical chemical reaction 1, following equation 2. A(g) is a gas phase molecule, * is the surface and *A is the adsorbed species on the surface.



$$\Delta G_{ads}^{*A} = G^{*A} - G_{(g)}^A - G^* \quad [2]$$

where

$$G^{*A} = E_{DFT}^{*A} + ZPE^{*A} - TS_{vib}^{*A} \quad [3]$$

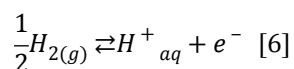
$$G_{(g)}^A = E_{DFT}^A + ZPE_{(g)}^A - TS_{trans, rot, vib(g)}^A \quad [4]$$

$$G^* = E_{DFT}^* \quad [5]$$

where E_{DFT}^x is the relative energy from the optimization extrapolated to 0 K (sigma \rightarrow 0) where x refers to either *A, A(g) or (*), ZPE is the zero-point energy and TS is the entropy contribution at 298.15 K. For the gas phase molecules, the entropy includes all the contributions, translational, rotational and vibrational, and was obtained from standard thermodynamic tables.¹¹ For the adsorbed species, the entropy includes only the vibrational contributions and it was calculated using statistical mechanical equations within the harmonic oscillator approximation.¹² These contributions were obtained by performing a vibrational analysis within the VASP code using the finite differences method. Within this method only the adsorbed species are displaced in all directions while the slab is kept fixed.

To obtain the solution phase free energy of water from the DFT calculated gas phase water we corrected the energy by adding -0.087 eV to the TS term.¹³ This represents the difference between the free energy of formation of gas phase water and liquid phase water at 298.15 K.

The potential dependence of all the proton-coupled electron transfer reactions was calculated using the computational hydrogen electrode (CHE) model,¹³ where at equilibrium and standard conditions (0V and a pressure of 1 atm), the protons in solution and the electrons in the electrode ($H^+(aq)$, e^-) are in equilibrium with $H_2(g)$, as shown in the following chemical equation:

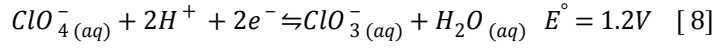
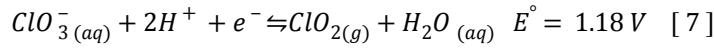


With this thermodynamic fact we can overcome the computational difficulty of calculating the energy of protons and electrons in DFT and instead calculate the ground state free energy of a $H_2(g)$ molecule. Half of that energy will then represent the free energy of the coupled proton and electron as shown in eq [6].^{13,14}

The solution phase free energy of perchlorate, sulfate and bisulfate anions were calculated via a thermodynamic cycle combining DFT free energies and tabulated experimental standard redox chemical potentials at standard conditions (298.15 K and 1 atm), as a direct calculation of these anion free energies would be difficult with DFT due to the long length and time scales of the solvation energetics. Using an electrochemical thermodynamic cycle allows us to calculate the solution phase free energy of an anion from a neutral, typically gas phase, species, such that its energy can be accurately determined with DFT as $G = ZPE - TS + PV$. This is analogous to the computational hydrogen electrode method, except it requires experimentally measured equilibrium potentials, whereas in the computational hydrogen electrode method, the equilibrium potential between hydrogen gas and aqueous protons at standard conditions is defined to be exactly 0 V, i.e., $G^{e^-} = -n |e| U^\circ = 0$.

As an example, the solution phase free energy of $ClO_4^-(aq)$ will be discussed below.

Using the following redox equations at standard conditions, we can use the calculated free energy of $ClO_2(g)$ to calculate the free energy of aqueous perchlorate.



From the equation 7, the $\text{ClO}_3^- (aq)$ free energy can be determined, which can then be used in equation 8 to determine the solution phase free energy of $\text{ClO}_4^- (aq)$. Note that the free energy of the electron is $G^{e^-} = -n|e|U^\circ$ and the total free energy is $\Delta G = \Delta G^\circ - k_b T \ln(10) \text{ pH}$, where the second term of the equation is 0 at $\text{pH} = 0$ and at equilibrium $\Delta G = 0$. Therefore,

The free energy of equation 7 is

$$\Delta G = G_{(g)}^{\text{ClO}_2} + G_{(aq)}^{\text{H}_2\text{O}} - G_{(aq)}^{\text{ClO}_3^-} - G_{(g)}^{\text{H}_2} - G^{e^-} \quad [9]$$

Substituting $G^{e^-} = -n|e|U^\circ$, and $E^\circ = U^\circ$:

$$G_{(aq)}^{\text{ClO}_3^-} = G_{(g)}^{\text{ClO}_2} + G_{(aq)}^{\text{H}_2\text{O}} - G_{(g)}^{\text{H}_2} - (-n|e|U^\circ) \quad [10]$$

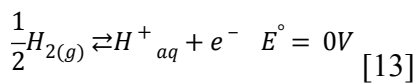
$$G_{(aq)}^{\text{ClO}_3^-} = G_{(g)}^{\text{ClO}_2} + G_{(aq)}^{\text{H}_2\text{O}} - G_{(g)}^{\text{H}_2} + 1.18 \text{ eV} \quad [11]$$

Similarly,

$$G_{(aq)}^{\text{ClO}_4^-} = G_{(aq)}^{\text{ClO}_3^-} + G_{(aq)}^{\text{H}_2\text{O}} - G_{(g)}^{\text{H}_2} + 2.4 \text{ eV} \quad [12]$$

Now, the free energy of the proton in solution is calculated following the definition that the standard hydrogen redox potential is set to 0 V on the NHE scale.

Given the previous definitions:



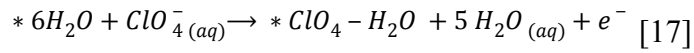
$$\Delta G = G_{(aq)}^{\text{H}^+} - n|e|U - \frac{1}{2}G_{(g)}^{\text{H}_2} \quad [14]$$

Then,

$$0 = G_{(aq)}^{H^+} - 1 * e(0V) - \frac{1}{2} G_{(g)}^{H_2} \quad [15]$$

$$\frac{1}{2} G_{(g)}^{H_2} = G_{(aq)}^{H^+} \quad [16]$$

Then, the adsorption energy of perchlorate on the surface is calculated as follows: Given the following reaction, where we used an adsorbed water adlayer as the reference state *6 H₂O then,



*ClO₄ - H₂O represents the adsorbed perchlorate coadsorbed with one water molecule. Then, we can determine the change in free energy of adsorption of adsorbed solvated perchlorate as shown below in eq 18.

$$\Delta G_{ads}^{*ClO_4 - H_2O} = G^{*ClO_4 - H_2O} + 5G_{(aq)}^{H_2O} - G^{*6H_2O} - G_{(aq)}^{ClO_4^-} - n|e|U \quad [18]$$

which represents the energy of adsorption of perchlorate ion on a surface covered with 2/3 ML water molecules, perturbing the water adlayer and displacing water molecules after its adsorption. In our case the adsorbed perchlorate is solvated with one water molecule.

Adsorption free energies of *OH, *H and *O

Adsorption of hydroxide and water adlayer

The adsorption energy of *OH was calculated within a water bilayer, which constitutes explicit solvation. In this study we used a single water bilayer with a total water species coverage of 2/3 ML, and varied the hydroxide (*OH+*H₂O) coverage by removing hydrogen from the adlayer. The single water bilayer structure of $\sqrt{3} \times \sqrt{3} R30^\circ$ has been found to be

stable on closed packed metal surfaces.¹⁵⁻¹⁷ Furthermore the good match between the lattice constant of metals and the water layer makes this model attractive for computational electrocatalysis as a good approximation to account for solvation effects,^{13,18-21} especially those coming from the first solvation shell.

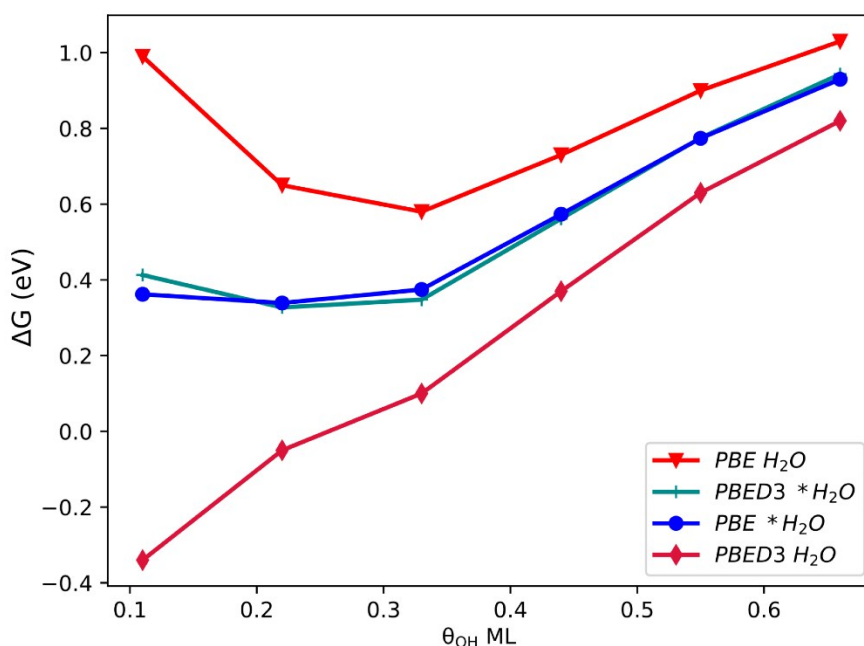
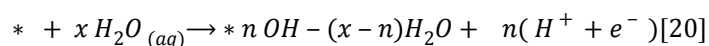
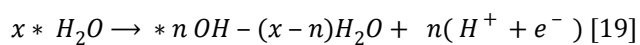


Figure S7. Hydroxide *OH free energy of adsorption as a function of coverage on Pd_{ML}Pt(111) calculated at the PBE and PBED3 level of theory. The plotted adsorption energy is calculated with two different reference states: from the adsorbed water bilayer (*H₂O) and from solution phase water (H₂O).

We can calculate the adsorption energy of *OH in two ways, (i) by using the adsorbed water bilayer as the reference state^{18,22} using eq 19 and (ii) by using solution phase water as the reference state using eq 20.



In both cases $x = 6$. Figure S7 shows the adsorption energy of $*OH$ as a function of $*OH$ coverage calculated from either solution phase (H_2O (aq)) or adsorbed water bilayer ($*H_2O$) as reference state and with and without dispersion corrections for both cases.

We observe that:

- 1) when referencing adsorbed water, for PBE and PBED3 the adsorption energies are basically the same and do not differ by more than $0.05 (\pm 0.02)$ eV, see Table S1 OH (b) and Figure S7 cyan (PBED3) and blue lines (PBE);
- 2) when referencing solution phase water with PBE, the energies are less favorable (red triangles) than those calculated with PBED3 (velvet diamonds). The difference between these two at the lowest coverage is ~ 1.32 eV and
- 3) as the $*OH$ coverage increases, the energies tend to converge and do not differ by more than ~ 0.2 eV independent of the reference state.

As the water-metal interactions are most effected by vdW interactions,^{23,24} the strong promotion of the adsorption of $*OH+*H_2O$ at low $*OH$ coverage, and weaker promotion at high $*OH$ coverage (relative to that calculated without vdW corrections) is simply proportional to the amount of water present in the $*OH+*H_2O$ bilayer. This effect is roughly canceled when using an adsorbed water reference state.

Similarly to case 1, the adsorption thermodynamics of the water adlayer on Pt(111) relative to that on $Pd_{ML}Pt(111)$ with vdW corrections does not significantly differ from that obtained without the vdW corrections, in fact the difference in binding strength with vs. without vdW corrections between the two surfaces is ~ 0.03 eV, with stronger adsorption on $Pd_{ML}Pt(111)$. This is because the stabilization incorporated by the vdW corrections for both surfaces is of the same magnitude, ~ 0.24 eV. Thus, the effect of including vdW corrections is also canceled when using adsorbed water as a reference state in the calculation of our adsorption

potentials. In this way the impact of vdW corrections is minimal as shown in Figure S7 on Pd_{ML}Pt(111).

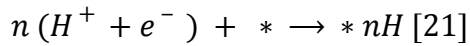
In either case, an appropriate representation of water adsorption is necessary for obtaining accurate DFT adsorption potentials.

Table S1: Free energies of adsorption in eV for 1/3 ML coverage of *H, *O and 1/3*OH-1/3 *H₂O (PBE and PBED3). Using (a) solution phase water and (b) adsorbed water bilayer as the reference state.

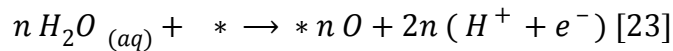
	PBE		PBED3	
	Pd _{ML} Pt(111)	Pt(111)	Pd _{ML} Pt(111)	Pt(111)
*H	-0.35	-0.29	-0.45	-0.39
*OH (a)	0.66	0.71	0.10	0.20
*OH (b)	0.37	0.43	0.35	0.39
*O	1.25	1.46	1.11	1.31

Adsorption of hydrogen and oxygen

The free energies of adsorption of *H, *O were calculated at different coverages using the same 3x3 unit cell by the following equations:



$$\Delta G_{ads}^{*H} = \frac{G(*nH) - \frac{n}{2}G_{(g)}^{H_2} - G^*}{n} \quad [22]$$



$$\Delta G_{ads}^{*O} = \frac{G^{*nO} + 2n \frac{1}{2} G_{(g)}^{H_2} - n G_{(aq)}^{H_2O} + G^*}{n} [24]$$

Where (*) is the surface, *H and *O are the adsorbed species, n equals the number of adsorbed species per unit cell, G(*) is the free energy of the isolated slab.

The adsorption of *H and *O were calculated at their most stable sites (fcc) in both cases, and without explicit solvation following the equations 22 and 24.

Free energies vs. coverage diagrams

Pd_{ML}Pt(111) Phase Diagrams

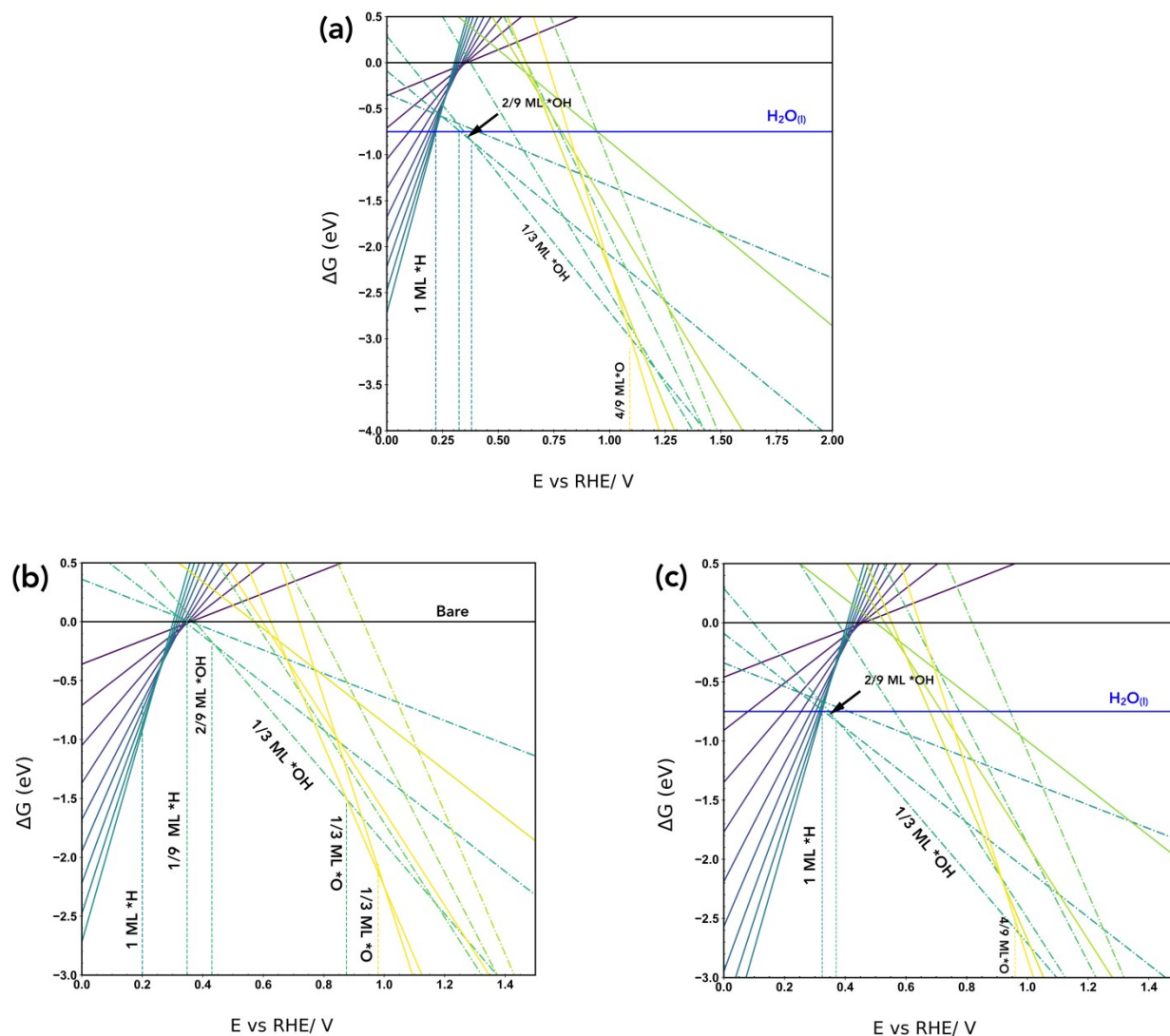


Figure S8. Calculated free energies of

adsorption for Pd_{ML}Pt(111) as a function of potential vs RHE using three different methods. Method 1, shown in (a), where the adsorption potentials of hydroxide are calculated from solution phase water with PBED3, as shown in equation 20, while the adsorption potentials of hydrogen and oxygen are calculated with PBE. Method 2, shown in (b), the adsorption potentials are calculated with PBE and the reference state for *OH adsorption is the adsorbed water adlayer, as shown in equation 19. Method 3, shown in (c), the adsorption potentials are

calculated with PBED3 and solution phase water is used as the reference state, as shown in equation 20.

Pt(111) Phase Diagrams

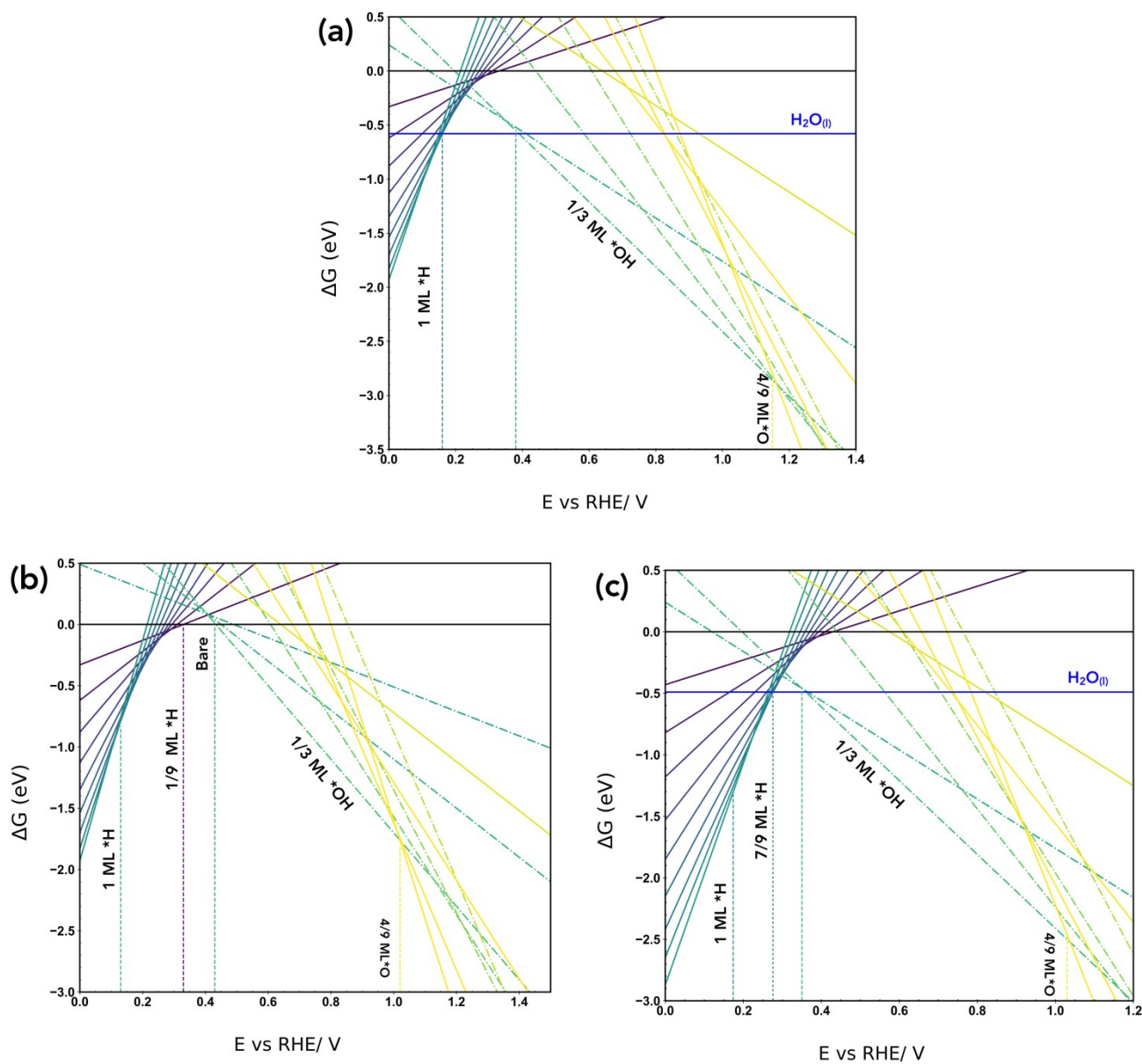


Figure S9. Calculated free energies of adsorption for Pd_{ML}Pt(111) as a function of potential vs RHE using three different methods. Method 1, shown in (a), where the adsorption potentials of hydroxide are calculated from solution phase water with PBED3, as shown in equation 20, while the adsorption potentials of hydrogen and oxygen are calculated with

PBE. Method 2, shown in (b), the adsorption potentials are calculated with PBE and the reference state for *OH adsorption is the adsorbed water adlayer, as shown in equation 19.

Method 3, shown in (c), the adsorption potentials are calculated with PBED3 and solution phase water is used as the reference state, as shown in equation 20.

References

- 1 R. Hoyer, L. A. Kibler and D. M. Kolb, *Electrochi. Acta*, 2003, **49**, 63–72.
- 2 M. P. Soriaga, J. Stickney, L. A. Bottomley and Y.-G. Kim, Eds., *Thin Films: Preparation, Characterization, Applications*, Springer US, 2002.
- 3 M. Arenz, V. Stamenkovic, T. J. Schmidt, K. Wandelt, P. N. Ross and N. M. Markovic, *Surf. Sci.*, 2003, **523**, 199–209.
- 4 G. Kresse and J. Furthmüller, *Phys. Rev. B*, 1996, **54**, 11169–11186.
- 5 J. P. Perdew, K. Burke and M. Ernzerhof, *Phys. Rev. Lett.*, 1996, **77**, 3865–3868.
- 6 G. Kresse and D. Joubert, *Phys. Rev. B*, 1999, **59**, 1758–1775.
- 7 H. J. Monkhorst and J. D. Pack, *Phys. Rev. B*, 1976, **13**, 5188–5192.
- 8 S. Grimme, J. Antony, S. Ehrlich and H. Krieg, *J. Chem. Phys.*, 2010, **132**, 154104.
- 9 S. Grimme, S. Ehrlich and L. Goerigk, *J. Comput. Chem.*, 2011, **32**, 1456–1465.
- 10 M. Methfessel and A. T. Paxton, *Phys. Rev. B*, 1989, **40**, 3616–3621.
- 11 M. W. Chase, C. A. Davies, J. R. Downey, D. J. Frurip, R. A. MacDonald and A. N. Syverud, *J. Phys. Chem. Ref. Data*, 1985, **Suppl. 1 to Vol. 14**, 1856.
- 12 B. Fultz, *Prog. Mater. Sci.*, 2010, **55**, 247–352.
- 13 J. K. Nørskov, J. Rossmeisl, A. Logadottir, L. Lindqvist, J. R. Kitchin, T. Bligaard and H. Jónsson, *J. Phys. Chem. B*, 2004, **108**, 17886–17892.
- 14 F. Calle-Vallejo and M. T. M. Koper, *Electrochimica Acta*, 2012, **84**, 3–11.
- 15 H. Ogasawara, B. Brena, D. Nordlund, M. Nyberg, A. Pelmenschikov, L. G. M. Pettersson and A. Nilsson, *Phys. Rev. Lett.*, 2002, **89**, 276102.
- 16 S. Schnur and A. Groß, *New J. Phys.*, 2009, **11**, 125003.
- 17 A. Michaelides and P. Hu, *J. Am. Chem. Soc.*, 2001, **123**, 4235–4242.
- 18 Z.-D. He, S. Hanselman, Y.-X. Chen, M. T. M. Koper and F. Calle-Vallejo, *J. Phys. Chem. Lett.*, 2017, **8**, 2243–2246.
- 19 I. T. McCrum and M. J. Janik, *J. Phys. Chem. C*, 2016, **120**, 457–471.
- 20 T. Roman and A. Groß, *Catal. Today*, 2013, **202**, 183–190.
- 21 L. P. Granda-Marulanda, S. Builes, M. T. M. Koper and F. Calle-Vallejo, *ChemPhysChem*, 2019, **20**, 1-6.
- 22 I. T. McCrum, M. A. Hickner and M. J. Janik, *Langmuir*, 2017, **33**, 7043–7052.
- 23 K. Forster-Tonigold and A. Groß, *J. Chem. Phys.*, 2014, **141**, 064501.
- 24 J. Carrasco, J. Klimeš and A. Michaelides, *J. Chem. Phys.*, 2013, **138**, 024708.